Axion-pion thermalization rate in unitarized NLO chiral perturbation theory

Luca Di Luzio,[1,2,*] Jorge Martin Camalich,[3,4,†] Guido Martinelli,[5,‡] José Antonio Oller,[6,§] and Gioacchino Piazza[7,‖]

[1]*Dipartimento di Fisica e Astronomia "G. Galilei", Università di Padova, Via F. Marzolo 8, 35131 Padova, Italy*
[2]*INFN Sezione di Padova, Via F. Marzolo 8, 35131 Padova, Italy*
[3]*Instituto de Astrofísica de Canarias, C/ Vía Láctea, s/n E38205-La Laguna, Tenerife, Spain*
[4]*Universidad de La Laguna, Departamento de Astrofísica-La Laguna, 38206 Tenerife, Spain*
[5]*Physics Department and INFN Sezione di Roma La Sapienza, Piazzale Aldo Moro 5, 00185 Roma, Italy*
[6]*Departamento de Física, Universidad de Murcia, E-30071 Murcia, Spain*
[7]*IJCLab, Pôle Théorie (Bât. 210), CNRS/IN2P3 et Université Paris-Saclay, 91405 Orsay, France*

(Received 20 December 2022; accepted 14 July 2023; published 17 August 2023)

We compute the axion-pion scattering $a\pi \to \pi\pi$, relevant for the axion thermalization rate in the early Universe, within unitarized next-to-leading-order chiral perturbation theory. The latter extends the range of validity of the chiral expansion of axion-pion scattering and thus provides a crucial ingredient for the reliable determination of the relic density of thermal axions, whenever the axion decoupling temperature is below that of the QCD phase transition. Implications for cosmological observables are briefly discussed.

DOI: 10.1103/PhysRevD.108.035025

I. INTRODUCTION

The QCD axion is a well-motivated new physics paradigm that provides at the same time a solution to the strong CP problem [1–4] and a cold dark matter candidate [5–8]. Additionally, a thermal population of relativistic axions [9], behaving as dark radiation or hot dark matter, might further contribute to the energy density of the Universe. Thermally produced axions can be probed by cosmic microwave background (CMB) experiments, such as the *Planck* satellite [10,11], as well as planned CMB Stage 4 (CMB-S4) surveys [12] which provide an observational window on the axion couplings to the Standard Model (SM) fields.

Depending on the axion decay constant f_a (or, equivalently, the axion mass $m_a \simeq 5.7 \times 10^6\ \mathrm{GeV}/f_a\ \mathrm{eV}$), whose inverse sets the strength of axion couplings, there are several processes stemming from the model-independent axion coupling to gluons, $\frac{\alpha_s}{8\pi}\frac{a}{f_a}G\tilde{G}$, which can keep the axion in thermal equilibrium with the SM thermal bath. For $m_a \lesssim 10$ meV, thermal axion production dominantly proceeds via its scatterings with gluons [13,14], corresponding to a decoupling temperature T_D above the GeV scale. On the other hand, for heavier axions one has $T_D \lesssim 1$ GeV and hence processes involving pions and nucleons must also be considered [15–17]. Although this transition region cannot be precisely determined due to the complications of the quark-hadron phase transition,[1] for axions approaching the eV scale the main thermalization channel is provided by the scattering $a\pi \to \pi\pi$ [16,17], with $T_D \lesssim T_c$, where $T_c \simeq 155$ MeV [20–22] is the QCD deconfinement temperature. The highest attainable axion mass from cosmological constraints on thermally produced axions is known as the axion hot dark matter bound (for recent analyses, see Refs. [23,24]), and it is mainly set by the axion-pion thermalization rate.

The scattering $a\pi \to \pi\pi$ can be computed at low energies within chiral perturbation theory (ChPT). The leading-order (LO) calculation was performed in Refs. [16,17], while Ref. [25] considered the impact of next-to-leading-order (NLO) corrections in order to assess the convergence of the chiral expansion. In this paper, we correct a mistake of Ref. [25] regarding the evaluation of the loop function in the NLO contribution. As discussed in the following, with the

*luca.diluzio@pd.infn.it
†jcamalich@iac.es
‡guido.martinelli@roma1.infn.it
§oller@um.es
‖gioacchino.piazza@ijclab.in2p3.fr

[1]It was recently proposed in Refs. [18,19] to interpolate the axion thermalization rate by matching the known high- and low-temperature asymptotic regions.

corrected result it can still be argued that the temperature where the chiral expansion of the axion-pion thermalization rate breaks down is $T_\chi \sim 70$ MeV, and hence it remains a crucial question to extend the validity of ChPT between T_χ and $T_c \simeq 155$ MeV. This is actually the main goal of the present work, that is, to extend the chiral description of axion-pion scattering above the validity region of standard ChPT, by employing a unitarization technique known as the inverse amplitude method (IAM) [26–28]. This method restores exact elastic unitarity attached to the so-called unitarity or right-handed cut of the amplitude, while preserving crossing symmetry perturbatively.

The paper is structured as follows. In Sec. II we recall the basic ingredients of the axion-pion chiral Lagrangian and update the NLO correction to axion-pion scattering in ChPT. In Sec. III we present the new calculation of the axion-pion scattering within unitarized NLO ChPT, whose impact on the axion-pion thermalization rate is subsequently discussed in Sec. IV. In Sec. V we discuss the convergence of the chiral expansion, while cosmological implications are considered in Sec. VI, and we finally conclude in Sec. VII. More technical details are deferred to a set of appendices.

II. AXION-PION SCATTERING IN ChPT

At the LO in the chiral expansion, the axion-pion effective Lagrangian is described by the contact interactions (see, e.g., Refs. [29,30])

$$\mathcal{L}^{\rm LO}_{a-\pi} \supset \frac{C_{a\pi}}{f_a f_\pi}\partial^\mu a[2\partial_\mu\pi^0\pi^+\pi^- - \pi^0\partial_\mu\pi^+\pi^- - \pi^0\pi^+\partial_\mu\pi^-] \tag{1}$$

and coupling strength

$$C_{a\pi} = \frac{1}{3}\left(\frac{m_d - m_u}{m_u + m_d} + c^0_d - c^0_u\right). \tag{2}$$

Here, $c^0_{u,d}$ are model-dependent coefficients which depend on the axion UV completion. For instance, $c^0_{u,d} = 0$ in the Kim-Shifman-Vainshtein-Zakharov model [31,32], while $c^0_u = \frac{1}{3}\cos^2\beta$ and $c^0_d = \frac{1}{3}\sin^2\beta$ in the Dine-Fischler-Srednicki-Zhitnitsky model [33,34], where $\tan\beta$ is the ratio between the vacuum expectation values of two-Higgs doublets.

For temperatures below the QCD phase transition, the main processes relevant for the axion thermalization rate are $a(p_1)\pi^0(p_2) \to \pi^+(p_3)\pi^-(p_4)$, whose amplitude at LO reads

$$\mathcal{M}^{\rm LO}_{a\pi^0\to\pi^+\pi^-} = \frac{C_{a\pi}}{f_\pi f_a}\frac{3}{2}[m_\pi^2 - s], \tag{3}$$

with $s = (p_1 + p_2)^2$, together with the crossed channels $a\pi^- \to \pi^0\pi^-$ and $a\pi^+ \to \pi^+\pi^0$. The amplitudes of the latter are obtained by replacing $s \leftrightarrow t = (p_1 - p_3)^2$ and $s \leftrightarrow u = (p_1 - p_4)^2$, respectively. Taking equal masses for the neutral and charged pions, one finds the squared matrix element (summed over the three channels above) [17]

$$\sum|\mathcal{M}|^2_{\rm LO} = \left(\frac{C_{a\pi}}{f_a f_\pi}\right)^2\frac{9}{4}[s^2 + t^2 + u^2 - 3m_\pi^4]. \tag{4}$$

The formulation of the axion-pion chiral Lagrangian including axion derivative terms at the NLO was worked out in Ref. [25] (see also Ref. [35]). The main ingredients are the axion-dressed $\mathcal{O}(p^4)$ terms of the standard chiral Lagrangian [36] and the NLO pion axial current to which the axion couples derivatively. A nontrivial aspect, compared to the standard two-flavor chiral Lagrangian, consists in the mixing between the axion and the neutral pion, which can be dealt with either by diagonalizing the axion-pion propagator at the NLO or by explicitly retaining the mixing in the Lehmann-Symanzik-Zimmermann reduction formula [37] for the $a\pi \to \pi\pi$ scattering amplitude. For more details, we refer the reader directly to Ref. [25].

However, Ref. [25] contained a mistake in the loop function of the NLO scattering amplitude, related to a wrong choice of the branch cut of the two-point unitary loop function that affects the results for negative u and t. The corrected $a\pi^0 \to \pi^+\pi^-$ NLO amplitude is given in Appendix A, together with that for $a\pi^0 \to \pi^0\pi^0$ which enters the cross section only at next-to-next-to-leading order (NNLO) (as this channel is absent at LO), but which will be needed for the nonperturbative unitarization method of the NLO ChPT $a\pi \to \pi\pi$ amplitudes to be discussed in Sec. III.

For the numerical evaluation of the perturbative ChPT rates discussed in this work we use the central values of the standard low-energy constants (LECs): $\overline{\ell_1} = -0.36(59)$ [38], $\overline{\ell_2} = 4.31(11)$ [38], $\overline{\ell_3} = 3.53(26)$ [39], $\overline{\ell_4} = 4.73(10)$ [39], $\ell_7 = 7(4)\times 10^{-3}$ [40], along with $m_u/m_d = 0.50(2)$ [39], $f_\pi = 92.1(8)$ MeV [41], and $m_\pi = 137$ MeV (corresponding to the average neutral/charged pion mass).

III. UNITARIZED AXION-PION SCATTERING

Partial-wave amplitudes (PWAs) are the most adequate method to impose unitarity constraints on amplitudes at low energies. As it is also conventional in studies of $\pi\pi$ scattering, we start our analysis by projecting the amplitudes $\mathcal{M}$ from the charge basis to a basis with well-defined total isospin I, giving rise to the amplitudes A_I. For $a\pi^0 \to \pi^+\pi^-$ and $a\pi^0 \to \pi^0\pi^0$ scattering (see Appendix B for conventions),

$$A_0 = -\frac{1}{\sqrt{3}}(2\mathcal{M}_{+-} + \mathcal{M}_{00}),$$
$$A_2 = \sqrt{\frac{2}{3}}(\mathcal{M}_{00} - \mathcal{M}_{+-}), \tag{5}$$

where we have simplified the notation by indicating the charges of the two final pions as subscripts of the amplitudes in the charge basis. We have also used the fact that $\mathcal{M}_{+-} = \mathcal{M}_{-+}$ because of charge-conjugation symmetry.

For $a\pi^+ \to \pi^0\pi^+$ scattering,

$$A_1 = -\frac{1}{\sqrt{2}}(\mathcal{M}_{+0} - \mathcal{M}_{0+}),$$
$$A_2{}' = -\frac{1}{\sqrt{2}}(\mathcal{M}_{+0} + \mathcal{M}_{0+}). \tag{6}$$

The amplitudes with definite isospin for $a\pi^- \to \pi^0\pi^-$ differ from A_1 and A_2' only by a global minus sign. Note that A_2 and A_2' are different because the coupling of the axion with pions violates isospin.

The projection of these amplitudes into a basis of states with well-defined total angular momentum J is obtained by means of the usual formulas for the PWAs of the scattering of spin-zero particles,

$$A_{IJ}(s) = \frac{1}{2}\int_{-1}^{+1} dx P_J(x) A_I(s,x),$$
$$A_I(s,x) = \sum_{J=0}^{\infty}(2J+1)P_J(x)A_{IJ}(s). \tag{7}$$

As long as inelasticities in $a\pi \to \pi\pi$ scattering can be neglected (see discussion below), unitarity implies the following algebraic constraint for its PWAs [28,42]:

$$\mathrm{Im}\, A_{IJ}(s) = \frac{\sigma(s)}{32\pi} A_{IJ}(s) T^*_{IJ}(s)\theta(s-4m_\pi^2), \tag{8}$$

where $\sigma(s)$ is the phase-space factor defined below Eq. (A1) and $T_{IJ}(s)$ are the *strong* PWAs of $\pi\pi$ scattering in the isospin basis. In Eq. (8) we are using the conventions for the normalization of the states in Appendix B and have included a Bose-symmetric factor of $1/2$ that appears in the isospin basis. From the unitarity relation it follows that the continuous phases of $A_{IJ}(s)$ and $T_{IJ}(s)$ (i.e., *phase shifts*) are the same, which is Watson's theorem for final-state interactions [43].

Unitarity is fulfilled only perturbatively in ChPT. Indeed, if we denote the amplitudes calculated up to $\mathcal{O}(p^{2n})$ in the chiral expansion by $A_{IJ}^{(2n)}$ and $T_{IJ}^{(2n)}$, then Eq. (8) implies[2]

$$\mathrm{Im}\, A_{IJ}^{(4)}(s) = \frac{\sigma(s)}{32\pi} A_{IJ}^{(2)}(s) T_{IJ}^{(2)}(s)\theta(s-4m_\pi^2). \tag{9}$$

Different methods have been proposed to impose exact elastic unitarity in scattering amplitudes that match the perturbative ChPT predictions at low energies. These have seen multiple applications and led to very significant progress in the understanding of the hadronic phenomena (see Refs. [28,42,44,45] for recent reviews). In fact, $\pi\pi$ scattering, with the characterization of the σ or $f_0(500)$ resonance, stands as one of the first successful applications of these methods [28,44,46–49]. Given that the unitary corrections to the ChPT NLO calculation of $a\pi \to \pi\pi$ scattering will be given by the pion's final-state interactions, we expect the unitarization methods to provide a realistic amplitude in the energy region relevant for the axion hot dark matter bound.

In our analysis we focus on the IAM technique which adopts the form

$$A_{IJ}(s) = \frac{A_{IJ}^{(2)}(s)}{1 - A_{IJ}^{(4)}(s)/A_{IJ}^{(2)}(s)} \tag{10}$$

and can also be regarded as a Padé approximant of the NLO ChPT amplitude [50]. The IAM formula can be formally derived using a dispersion relation [27,28,51,52] and the different caveats and uncertainties of the method have been thoroughly studied in Ref. [53]. One particular caveat concerns the validity of the two-body unitarity relation for s above the four-pion threshold. However, as discussed and estimated quantitatively for $\pi\pi$ scattering in Ref. [53], these inelastic contributions to the imaginary part are suppressed and can be neglected for the energies of interest.

An obvious benefit of expanding the inverse of the A_{IJ} instead of the latter is that A_{IJ}^{-1} has a zero at a resonance pole, while A_{IJ} becomes infinity. This makes the IAM, in the form (10), a suitable method to address resonance dynamics below the chiral expansion scale $\Lambda_{\mathrm{ChSB}} \simeq 4\pi f_\pi$ [53]. This is also reflected in the two-body elastic unitarity relation for the inverse amplitude, which reads

$$\mathrm{Im}\, A_{IJ}^{-1}(s) = -\frac{\sigma(s)}{32\pi}\frac{T_{IJ}(s)}{A_{IJ}(s)}, \tag{11}$$

as can be easily deduced from Eq. (8). Therefore, a resonance pole, which appears in both T_{IJ} and A_{IJ}, cancels in their ratio.

For our analysis we implement the IAM for the PWAs in the S wave ($J=0$, $I=0$, 2) and P wave ($J=1$, $I=1$). The cases ($I=J=0$, 1) are of special interest since they correspond to the quantum numbers of the prominent $f_0(500)$ (also known as σ) and $\rho(770)$ resonances [54], respectively, leading to large (unitarity) corrections to $\pi\pi$ scattering in the low-energy region of interest below 1 GeV.

[2]We have explicitly checked that the imaginary parts of our NLO results fulfill perturbative unitarity in the PWAs studied in this work.

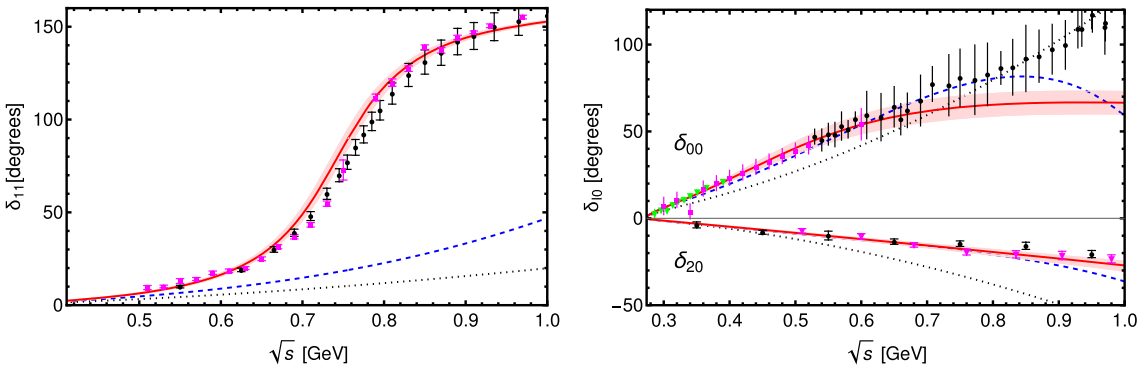

FIG. 1. Experimental data for the $\pi\pi \to \pi\pi$ phase shifts in the relevant channels compared to the theoretical $a\pi \to \pi\pi$ phase shifts in IAM (solid red), and the $\pi\pi \to \pi\pi$ predictions at LO ChPT (dotted black) and NLO ChPT (dashed blue). The IAM predictions include the 1σ confidence level regions that stem from the uncertainties in the LECs. The references for the data of the phase shifts for the $\pi\pi$ PWAs are given next: δ_{11}, Ref. [55] (pink squares) and Ref. [56] (black circles); δ_{20}, Ref. [57] (pink triangles) and Ref. [58] (black circles); δ_{00}, Ref. [59] (green triangles), Ref. [60] (pink squares), and the average data from Refs. [61–66] (black circles). The average procedure is explained in the δ_{11}^{00} subsection of Ref. [67].

The infinite tower of PWAs with $J \geq 2$ can be included perturbatively in ChPT. Indeed, we have checked that their contribution is only of a few percent relative to the S and P waves in the low-energy region. Therefore, we neglect them in the following.

In Fig. 1 we show the phase shifts $\delta_{IJ}(s)$ of the different $a\pi \to \pi\pi$ PWAs compared to the experimental data from $\pi\pi$ scattering, which should be identical as per Watson's theorem. Besides the prediction in the IAM, for comparison we show the $\pi\pi$ scattering phase shifts obtained from perturbative ChPT at LO and NLO. The latter is derived using the results in Ref. [36] and the standard values for the LECs introduced above in Sec. II. The perturbative expressions for the phase shifts are described in Appendix C. The LECs in IAM can be slightly different to those of ChPT. In particular, for the IAM calculations we use the combinations $\overline{\ell}_1 - \overline{\ell}_2 = -5.95(2)$, with $\overline{\ell}_1 + \overline{\ell}_2 = 4.9(6)$, determined from $\pi\pi$ scattering to fit the pole position and width of the ρ resonance precisely [46]. This is illustrated in the left panel of Fig. 1 by the good agreement of $\delta_{11}(s)$ with data across the resonance region.

For the case of the phase shifts of $a\pi^0$ scattering the IAM also agrees with the experimental data in both the $I = 0$ and $I = 2$ channels. In particular, the amplitudes describe the structure induced by the σ resonance in $\delta_{00}(s)$. As expected, the phase shifts obtained for the $a\pi$ scattering amplitudes are equivalent to those calculated in Ref. [46] for the $\pi\pi$ scattering amplitudes using the IAM. Note that the worsening of the agreement in δ_{00} starting at $\sqrt{s} \gtrsim 0.8$ GeV is an effect induced by the increase of the $f_0(980)$ resonance and the subsequent strong coupling to the $K\bar{K}$ channel with a prominent threshold effect [47,48,68], which are omitted in our $SU(2)$ analysis. In fact, our results for $\delta_{00}(s)$ are in very good agreement with those obtained in Ref. [69] by unitarizing $\pi\pi$ scattering calculated at NLO in $SU(2)$ ChPT. On the other hand, the energy range of applicability of the IAM framework can be in principle improved by unitarizing the coupled $\pi\pi$, $K\bar{K}$, and $\eta\eta$ interactions predicted by NLO SU(3) ChPT, as first shown in Ref. [70].

In the left panel of Fig. 2 we present our theoretical predictions for the $a\pi \to \pi\pi$ cross sections in the different channels of the charge basis, obtained in the IAM by inverting Eqs. (5)–(7). ChPT departs from the IAM results at low energies, $\sqrt{s} \simeq 0.5$ GeV. In the case of the $\pi^+\pi^-$ channel this is the typical scale at which unitarity corrections become large due to the σ resonance in the $I = J = 0$ channel. In the case of the $\pi^\pm\pi^0$ channel the disagreement is due to the prominent structure of the ρ resonance emerging in the amplitude.

In the right panel of Fig. 2 we show the predictions in IAM and ChPT for the sum of cross sections, which is the quantity most closely related to the thermal rate to be calculated in Sec. IV. NLO and higher-order corrections of size estimated by including the NNLO pieces (from the squared NLO contributions to the rate) start to get very large around $\sqrt{s} \simeq 0.6$ GeV. In Appendix B we present a more detailed comparison between ChPT at different orders and the IAM for the cross sections and also the absolute values of the PWAs.

IV. AXION-PION THERMALIZATION RATE

The axion-pion thermalization rate is defined via the phase-space integral [16,17]

$$\Gamma_a = \frac{1}{n_a^{\rm eq}} \int \frac{d^3\mathbf{p}_1}{(2\pi)^3 2E_1} \frac{d^3\mathbf{p}_2}{(2\pi)^3 2E_2} \frac{d^3\mathbf{p}_3}{(2\pi)^3 2E_3} \frac{d^3\mathbf{p}_4}{(2\pi)^3 2E_4} \times \sum |\mathcal{M}|^2 (2\pi)^4 \delta^4(p_1 + p_2 - p_3 - p_4) \times f_1 f_2 (1 + f_3)(1 + f_4), \tag{12}$$

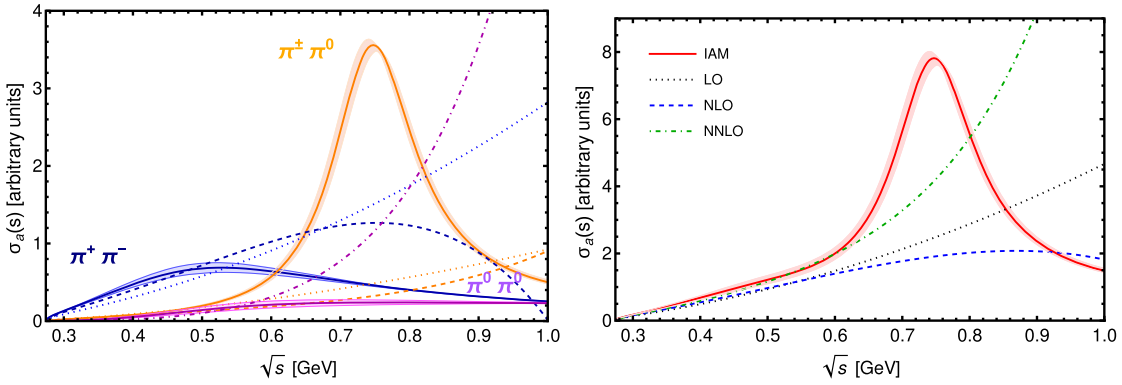

FIG. 2. Cross sections $\sigma_a(s)$ for axion-pion scattering in units of mb for $f_a = f_\pi$, so they scale as $\propto f_a^{-2}$. Left: plots for $a\pi^0 \to \pi^+\pi^-$ (blue), $a\pi^0 \to \pi^0\pi^0$ (magenta), and $a\pi^\pm \to \pi^\pm\pi^0$ (orange). Solid, dashed, and dotted lines are the predictions in IAM, NLO ChPT, and LO ChPT, respectively. We also include a dot-dashed magenta line describing the rate for the $a\pi^0 \to \pi^0\pi^0$ channel in ChPT which is a pure NLO contribution (the amplitude is zero at LO [25]). Right: sum of all the cross sections predicted in the IAM (solid, red) and in ChPT at LO (dotted, black), NLO (dashed, blue), and including the squared NLO pieces (NNLO) in the cross section (dot-dashed, green). Uncertainties in the IAM predictions are 1σ CL regions stemming from the errors in the LECs.

where $n_a^{\rm eq} = (\zeta_3/\pi^2)T^3$ and $f_i = 1/(e^{E_i/T} - 1)$. Here we neglect thermal corrections to the scattering matrix element, which is a good approximation for $T \lesssim m_\pi$ [71–73]. The integration of the thermal rate has been performed following the same procedure presented in Ref. [25] (see also Ref. [74]).

The perturbative result, $\Gamma_a = \Gamma_a^{\rm LO} + \Gamma_a^{\rm NLO}$, is obtained by expanding the amplitude squared in ChPT as $\sum|\mathcal{M}|^2 \simeq \sum|\mathcal{M}|^2_{\rm LO} + \sum 2{\rm Re}[\mathcal{M}_{\rm LO}\mathcal{M}^*_{\rm NLO}]$ and it can be cast in the following way:

$$\Gamma_a(T) = \left(\frac{C_{a\pi}}{f_a f_\pi}\right)^2 0.163T^5\left[h_{\rm LO}(m_\pi/T) - 0.251\frac{T^2}{f_\pi^2}h_{\rm NLO}(m_\pi/T)\right], \quad (13)$$

where the h functions are shown in Fig. 3. Note that we normalized $h_{\rm LO}(m_\pi/T_c) = h_{\rm NLO}(m_\pi/T_c) = 1$, with $m_\pi/T_c \simeq 0.88$. In fact, the h functions are meaningful only for $T \lesssim T_c$, since for higher temperatures pions are deconfined.

On the other hand, the thermal rate obtained via the unitarized IAM amplitude is given by

$$\Gamma_a^{\rm IAM}(T) = \left(\frac{C_{a\pi}}{f_a f_\pi}\right)^2 0.137T^5 h_{\rm IAM}(m_\pi/T), \quad (14)$$

where we factored out a T^5 dependence, which is characteristic of the LO ChPT rate. In order to compare the IAM result with the perturbative one (cf. Fig. 3), we also normalized $h_{\rm IAM}(m_\pi/T_c) = 1$.

The integrals in Eq. (12) cover a broad range of energies with contributions suppressed at high energies by the axion and pion Boltzmann factors. In order to assess the robustness of our predictions, especially at temperatures close to T_c, it is important to investigate the relative contributions to the thermal rate stemming from low energies $\sqrt{s} \lesssim 1$ GeV, which we deem the upper energy limit of applicability for IAM (for further qualifications, see Ref. [53]). In Fig. 4 we illustrate this by showing the temperature dependence of $\sqrt{s_{\rm MAX}}$ which is the cutoff (in $\sqrt{s}$) needed in Eq. (12) for the low-energy contribution to describe 70%, 80%, or 90% of the total thermal rate. By looking at the value of $\sqrt{s_{\rm MAX}}$ for $T \simeq T_c$ we find that 90% of the contribution to the thermal rates in IAM stem from the low-energy region for all of the temperatures of interest in our work.

In our analysis and in the parametrization shown in Eq. (14) we use the result of Γ_a obtained by cutting off the contributions in Eq. (12) at $\sqrt{s_{\rm MAX}} = 1$ GeV. Moreover, we estimate our theoretical error based on the difference between the thermal rates calculated within the IAM with and without cutoff.

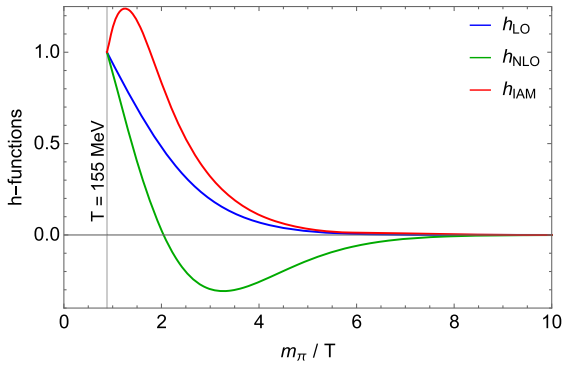

FIG. 3. Profile of the $h_{\rm LO}$, $h_{\rm NLO}$, and $h_{\rm IAM}$ functions, normalized to 1 at the value $m_\pi/T_c \simeq 0.88$.

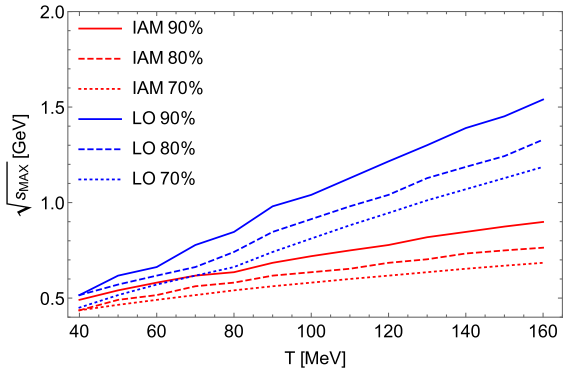

FIG. 4. Temperature dependence of $\sqrt{s_{\rm MAX}}$ at which it is sufficient to cut off the integration of the thermal rate in order to get 90%, 80%, and 70% of the total rate (without cutoff) for the LO and IAM cases. The plot shows the channel $\pi^+\pi^-$.

V. ON THE BREAKDOWN OF THE CHIRAL EXPANSION

In Ref. [25] the ratio between the NLO correction and the LO value of the axion-pion thermalization rate was taken as a criterion for the breakdown of ChPT, by requiring that $|\Gamma_a^{\rm NLO}/\Gamma_a^{\rm LO}| \lesssim 50\%$. However, it is more instructive to inspect the breakdown of ChPT at the levels of both cross sections and thermal rates, as well as for different final states separately. This analysis is summarized in Fig. 5. Starting from the ratio of cross sections in the left panel, we observe that for the $\pi^+\pi^0$ channel it reaches a maximal value of $\sim$40% around $\sqrt{s} \sim 0.6$ GeV, which agrees approximately with the energy at which NLO ChPT departs from the IAM prediction in Fig. 2. As discussed in Sec. III, this is due to large unitarity corrections and the emergence of the ρ resonance, which is ultimately the cause of the breakdown of the chiral expansion in the $I = J = 1$ channel at those energies. In the middle panel of Fig. 5 we show the temperature dependence of the ratio between the NLO and LO contributions to the thermal rates. In this case, the maximum is reached at $T_\chi \sim 70$ MeV that, according to our discussion for the cross sections, we interpret as the temperature at which ChPT breaks down. This correspondence between $\sqrt{s}$ and T can be supported by different semiquantitative arguments. For instance, by equating the NLO/LO ratio of cross sections and thermal rates given in Fig. 5, one gets the correlation between $\sqrt{s}$ and T shown in Fig. 6. We have also checked that alternative criteria, like, e.g., taking $\sqrt{s} \sim \langle E_\pi \rangle_T + \langle E_a \rangle_T$ in terms of the thermal average $\langle E \rangle_T = \rho(T)/n(T)$, give similar results.

Finally, in the right panel of Fig. 5 we show the ratio of the thermal rates between the results obtained with IAM and ChPT at LO. The differences in this case are more prominent and appear at lower temperatures. In fact, significant differences are visible even at $T = 20$ MeV for the $\pi^+\pi^-$ channel. However, this is not surprising given that a similar effect at threshold is known from $\pi\pi$ scattering. Indeed, higher-order corrections to the $I = J = 0$ $\pi\pi$ scattering length at LO are around 25% [75], which at the level of the cross sections implies a correction of around 50% near threshold.

VI. COSMOLOGICAL IMPLICATIONS

We next discuss the cosmological implications of the newly computed axion-pion thermalization rate. While an exhaustive treatment of cosmological observables is beyond the scope of this paper (for recent analyses, see Refs. [23,24]), here we focus on the axion contribution to the effective number of extra relativistic degrees of freedom [76],

$$\Delta N_{\rm eff} \simeq \frac{4}{7}\left(\frac{43}{4g_S(T_D)}\right)^{4/3}, \tag{15}$$

where $g_S(T_D)$ is the number of entropy degrees of freedom at the axion decoupling temperature T_D. The latter follows from the decoupling condition, $\Gamma_a(T_D) \simeq H(T_D)$,[3] in terms of the axion-pion thermalization rate in Eq. (12) and the Hubble rate, $H(T) = \sqrt{4\pi^3 g_\star(T)/45}T^2/m_{\rm pl}$ (assuming a radiation-dominated Universe), where $m_{\rm pl} = 1.22 \times 10^{19}$ GeV is the Planck mass and $g_\star(T)$ denotes the effective number of relativistic degrees of freedom. For the functions $g_S(T)$ and $g_\star(T)$ we employ the values provided by Ref. [77].

In the following, we set the model-dependent axion couplings to quarks in Eq. (2) to zero, i.e. $c^0_{u,d} = 0$, in order to represent the bound from $\Delta N_{\rm eff}$ as a function of m_a (the generalization to $c^0_{u,d} \neq 0$ is straightforward; see, e.g., Ref. [78]). The perturbative and unitarized rates are shown in Fig. 7 for the reference axion mass value $m_a = 0.3$ eV. For the IAM rate we employ a theoretical error that is based on the criterion discussed at the end of Sec. IV.

The bound of $\Delta N_{\rm eff}$ from *Planck* 2018 data [10,11] on the axion mass is finally displayed in Fig. 8, employing different approximations for the ChPT calculation of the axion-pion thermalization rate. With the IAM computation, valid up to temperatures approaching T_c, we can extract the conservative bound $m_a \lesssim 0.24$ eV.

To assess the impact of the high-energy discrepancy between the δ_{00} phase shift obtained from $\pi\pi$ data and the theoretical IAM prediction (see Fig. 1), we also compute the $\pi^+\pi^-$ and $\pi^0\pi^0$ rates by cutting off the energies above $\sqrt{s} \gtrsim 0.8$ GeV. Under this condition, the total rate is reduced by 10% at $T = 150$ MeV, with an error band reaching 11%, in comparison to the 7% represented by the

[3] A more refined determination of the axion thermal density, beyond the instantaneous decoupling approximation, would require the solution of the associated Boltzmann equation (see, e.g., Ref. [24]).

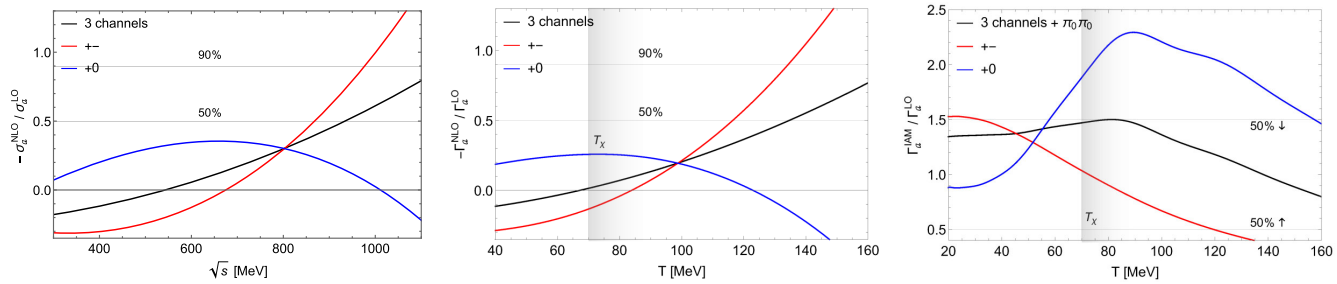

FIG. 5. Left (center): ratio between the NLO correction and LO axion-pion cross section (thermalization rate), considering the individual final-state channels $\pi^+\pi^-$ (red), $\pi^+\pi^0$, and $\pi^-\pi^0$ (blue, with the latter two being equal) and their sum (black). Right: ratio between the IAM (cutoff at 1 GeV) and LO thermalization rate.

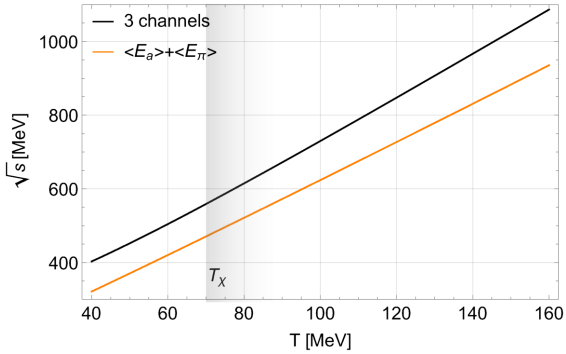

FIG. 6. $\sqrt{s}-T$ correspondence, using two different criteria: equating the % correction in the left and center panels of Fig. 5 (black line) and summing the axion-pion thermal energies in the initial state of the scattering (orange line).

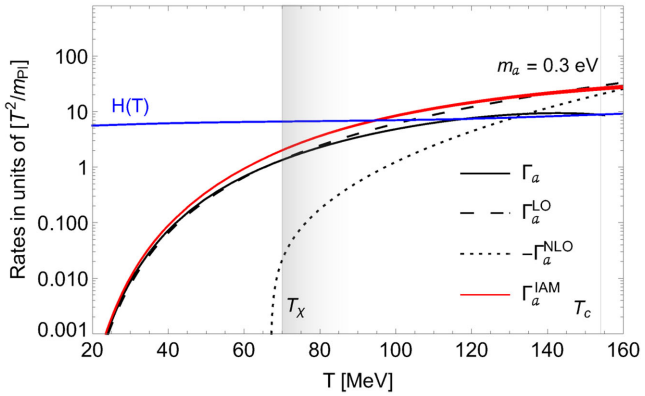

FIG. 7. Axion-pion thermalization rate vs Hubble rate (blue line) for $m_a = 0.3$ eV. The LO result, NLO correction, and total rate at NLO are denoted by the dashed, dotted, and solid black lines, respectively. In turn, the IAM rate is represented by a red band, where the upper line is the rate without a cutoff and the lower line is the rate cut off at $\sqrt{s} = 1$ GeV.

red band in Fig. 7. The corresponding hot dark matter bound would be $m_a \lesssim 0.25$ eV.

We remark that in the region between $m_a = 0.1$ and 1 eV axions transit from behaving as dark radiation to hot dark matter, so a more refined cosmological analysis would be

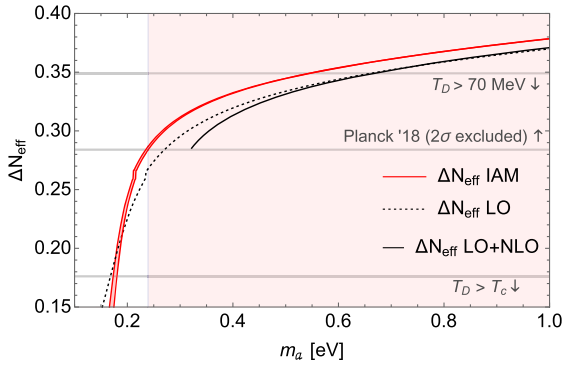

FIG. 8. $\Delta N_{\rm eff}$ as a function of m_a. The perturbative ChPT predictions are extrapolated for illustrative purposes beyond the temperature $T_\chi \sim 70$ MeV where the chiral expansion fails. The LO + NLO curve is stopped at $m_a = 0.31$ eV, corresponding to the minimum value of m_a for which the total rate at NLO intersects the Hubble rate.

needed in this intermediate regime. On the other hand, for $m_a \lesssim 0.3$ eV where the bound is extracted, the use of $\Delta N_{\rm eff}$ is still adequate (see, e.g., Fig. 1 in Ref. [23]). Finally, we note that the description in terms of axion dark radiation is well justified in the presence of model-dependent axion couplings $c^0_{u,d} \gg 1$ (as in some axion models [79]), since in order to keep $C_{a\pi}/f_a$ constant, the relevant mass window gets shifted to lower values of m_a, or in symmetry-based models where the axion mass is exponentially suppressed [80–82].

VII. CONCLUSIONS

The purpose of this work was twofold: to correct a mistake in Ref. [25] about the NLO correction to $a\pi \to \pi\pi$ scattering, and to extend the validity of the chiral description of axion-pion scattering by means of a unitarization method known as IAM. While the axion-pion thermalization rate can be computed within ChPT up to temperatures of $T_\chi \sim 70$ MeV, the unitarization method allows one to extend this further up to temperatures approaching the QCD deconfinement, $T_c \simeq 155$ MeV. The IAM rate shows

a sizable deviation from the perturbative one for temperatures $T \gtrsim 40$ MeV, corresponding to the contribution of the σ and ρ resonances in the region $\sqrt{s} \gtrsim 400$ MeV for axion-pion scattering.

Further improvements of particle physics aspects of the calculation of the axion thermal relic could stem from extending the analysis to three flavors which, as discussed in Sec. III, can start to produce large effects from energies $\sqrt{s} \simeq 800$ MeV and higher due to the kaon threshold and the appearance of the $f_0(980)$. As discussed in Sec. IV and illustrated in Fig. 4, these energies are only relevant for the higher temperatures, which could indeed become important to fully exploit future measurements of $\Delta N_{\rm eff}$ expected from the CMB-S4 experiments. In this context, one should also consider computing thermal corrections to the scattering amplitude (along the lines of the calculations done in Refs. [83,84]) and, eventually, develop techniques to describe axion thermal production in the intermediate region between $T_c \simeq 155$ MeV and 1 GeV.

ACKNOWLEDGMENTS

We thank Alessio Notari, Fabrizio Rompineve, and Giovanni Villadoro for useful discussions regarding Ref. [85]. The work of L. D. L. is supported by the project "CPV-Axion" under the Supporting TAlent in ReSearch@University of Padova (STARS@UNIPD) and by the INFN Iniziative Specifica APINE. The work of G. P. and L. D. L. has received funding from the European Union's Horizon 2020 research and innovation programme under the Marie Skłodowska-Curie Grant Agreement No. 860881. Work by J. M. C. is supported by PGC2018-102016-A-I00, and the "Ramón y Cajal" program RYC-2016-20672. Work by J. A. O. was partially supported by the MICINN AEI (Spain) Grant No. PID2019–106080 GB-C22/AEI/10.13039/501100011033, and by the EU Horizon 2020 research and innovation programme, STRONG-2020 project, under Grant agreement No. 824093.

Note added.—While completing this work, Ref. [85] appeared on the arXiv, where the validity of ChPT for axion-pion scattering is extended by using $\pi\pi$ scattering data via a rescaling of the corresponding cross sections. In Appendix D we provide a detailed comparison with the methodology of Ref. [85], in which we show that we obtain a reasonable agreement, up to subleading $\mathcal{O}(8\%)$ corrections in the calculation of the thermal rate.

APPENDIX A: NLO AMPLITUDES

The full analytical expression of the renormalized NLO amplitude for the $a\pi^0 \to \pi^+\pi^-$ process reads

$$\begin{aligned}\mathcal{M}^{\rm NLO}_{a\pi^0\to\pi^+\pi^-} = \frac{C_{a\pi}}{192\pi^2 f_\pi^3 f_a}\Bigg\{ & 15m_\pi^2(u+t) - 11u^2 - 8ut - 11t^2 - 6\overline{\ell_1}(m_\pi^2 - s)(2m_\pi^2 - s) \\ & - 6\overline{\ell_2}(-3m_\pi^2(u+t) + 4m_\pi^4 + u^2 + t^2) + 18\overline{\ell_4}m_\pi^2(m_\pi^2 - s) \\ & + 3\Bigg[3\sqrt{1-\frac{4m_\pi^2}{s}}s(m_\pi^2 - s)\ln\left(\frac{\sigma(s)-1}{\sigma(s)+1}\right) + \sqrt{1-\frac{4m_\pi^2}{t}}(m_\pi^2(t-4u) + 3m_\pi^4 + t(u-t))\ln\left(\frac{\sigma(t)-1}{\sigma(t)+1}\right) \\ & + \sqrt{1-\frac{4m_\pi^2}{u}}(m_\pi^2(u-4t) + 3m_\pi^4 + u(t-u))\ln\left(\frac{\sigma(u)-1}{\sigma(u)+1}\right)\Bigg]\Bigg\} - \frac{4\ell_7 m_\pi^2 m_d(s-2m_\pi^2)m_u(m_d-m_u)}{f_\pi^3 f_a(m_d+m_u)^3}, \end{aligned} \tag{A1}$$

where $\sigma(s) = (1 - 4m_\pi^2/s)^{1/2}$. Note that the term proportional to $\bar{\ell}_4$ in the second row arises from the NLO correction to f_π in the LO amplitude (see, e.g., Ref. [36]). The amplitudes for the crossed channels $a\pi^- \to \pi^0\pi^-$ and $a\pi^+ \to \pi^+\pi^0$ are obtained by cross symmetry through the replacements $s \leftrightarrow t$ and $s \leftrightarrow u$, respectively. Similarly, for the $a\pi^0 \to \pi^0\pi^0$ amplitude that is needed for the IAM unitarization method we obtain

$$\begin{aligned}\mathcal{M}_{a\pi^0\to\pi^0\pi^0} = \frac{3C_{a\pi}}{96\pi^2 f_\pi^3 f_a}\Bigg\{ & -2(\overline{\ell_1} + 2\overline{\ell_2} + 3)(3m_\pi^4 - 3m_\pi^2(t+u) + t^2 + tu + u^2) - 3\Bigg(\sqrt{1-\frac{4m_\pi^2}{s}}(m_\pi^2 - s)^2\ln\left(\frac{\sigma(s)-1}{\sigma(s)+1}\right) \\ & + \sqrt{1-\frac{4m_\pi^2}{t}}(m_\pi^2 - t)^2\ln\left(\frac{\sigma(t)-1}{\sigma(t)+1}\right) + \sqrt{1-\frac{4m_\pi^2}{u}}(m_\pi^2 - u)^2\ln\left(\frac{\sigma(u)-1}{\sigma(u)+1}\right)\Bigg)\Bigg\} + \frac{36\ell_7 m_\pi^4 m_d m_u(m_d - m_u)}{f_\pi^3 f_a(m_d+m_u)^3}. \end{aligned} \tag{A2}$$

APPENDIX B: CONVENTIONS AND DETAILS OF THE IAM ANALYSIS

The IAM analysis is performed at the level of PWAs, which requires the relations between $\pi\pi$ states in the isospin basis, labeled as $|II_3\rangle$ for total isospin I and third component I_3, and the charge basis. For the $\pi^+\pi^-$ final state,

$$|00\rangle = -\frac{1}{\sqrt{3}}(|\pi^+\pi^-\rangle + |\pi^-\pi^+\rangle + |\pi^0\pi^0\rangle),$$
$$|20\rangle = \frac{1}{\sqrt{6}}(2|\pi^0\pi^0\rangle - |\pi^+\pi^-\rangle - |\pi^-\pi^+\rangle). \quad \text{(B1)}$$

For the $\pi^\pm\pi^0$ final state,

$$|2 \pm 1\rangle = \mp\frac{1}{\sqrt{2}}(|\pi^\pm\pi^0\rangle + |\pi^0\pi^\pm\rangle),$$
$$|1 \pm 1\rangle = \mp\frac{1}{\sqrt{2}}(|\pi^\pm\pi^0\rangle - |\pi^0\pi^\pm\rangle). \quad \text{(B2)}$$

These relations have been used to project the chiral amplitudes (given in the charge basis) onto the isospin basis, leading to Eqs. (5) and (6).

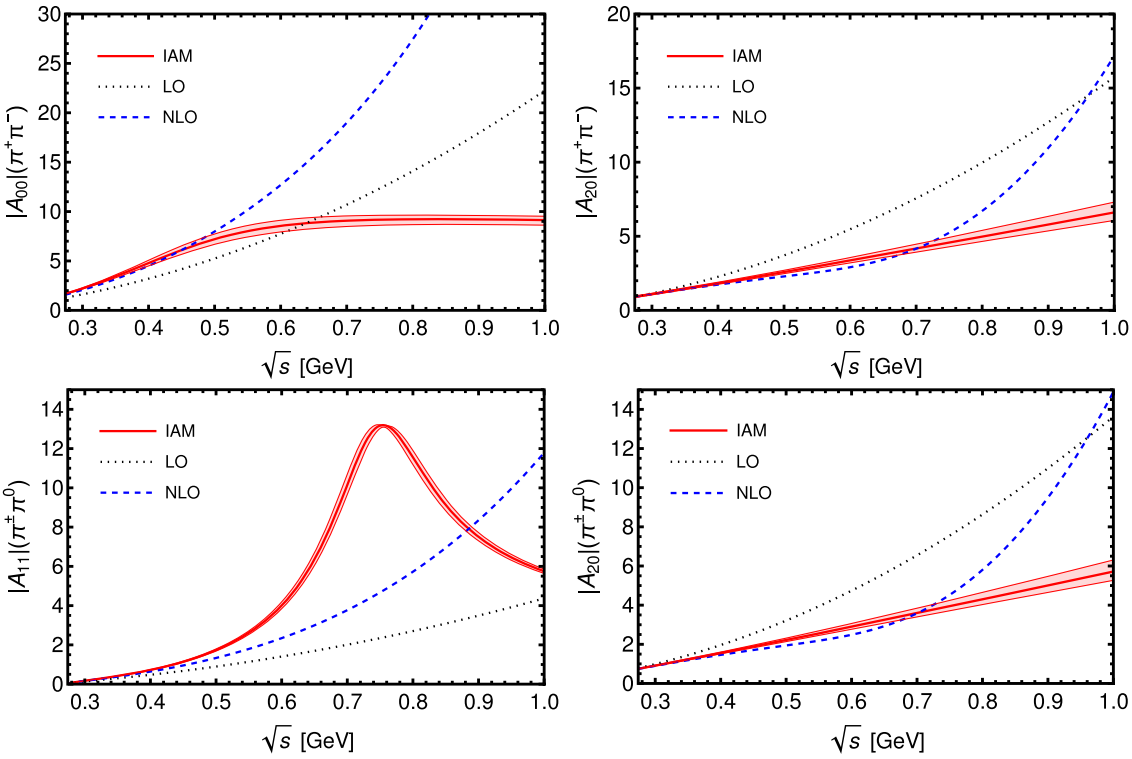

FIG. 9. Absolute values of the PWAs in the different isospin and angular momentum channels considered in this work. The predictions in IAM, ChPT at LO, and ChPT at NLO are shown by solid (red), dotted (black), and dashed (blue) lines, respectively. Error bands at 1σ in the IAM stem from uncertainties in the LECs.

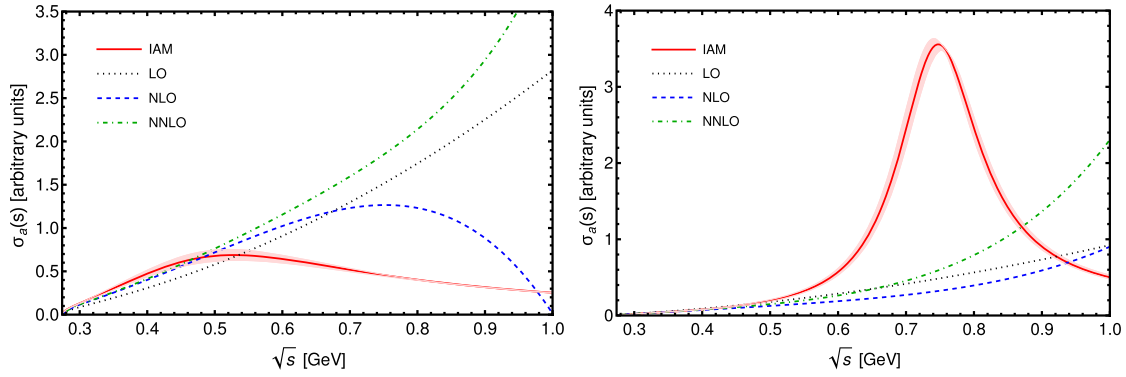

FIG. 10. Cross sections of the $a\pi^0 \to \pi^+\pi^-$ (left) and $a\pi^+ \to \pi^0\pi^+$ (right) channels predicted by the IAM (solid, red) and in ChPT at LO (dotted, black), NLO (dashed, blue), and including NNLO pieces (dot-dashed, green). Uncertainties in the IAM predictions are 1σ CL regions stemming from the errors in the LECs.

In the following we present additional results comparing the different amplitudes included in our analysis. In Fig. 9 we show the absolute values of the PWAs in ChPT at LO (black dotted lines), at NLO (blue dashed lines), and in the IAM (red solid lines). In turn, in Fig. 10 we show the contributions to the cross sections in separate channels (in the charge basis) contributing to the thermal rate. Besides the results in IAM (red solid lines), we show the ones in ChPT at LO (black dotted lines), contributing to the cross section like LO^2, NLO (blue dashed lines), also adding to the latter the LO-NLO interference terms and, finally, also adding the NNLO contributions to the rates (green dot-dashed lines).

APPENDIX C: CHPT EXPRESSIONS OF PHASE SHIFTS

Let us describe a given $a\pi \to \pi\pi$ PWA (omitting indices I and J) in ChPT up to NLO as

$$A = A_2 + \mathrm{Re}(A_4) + i\rho T_2 A_2, \tag{C1}$$

where we have labeled the amplitudes by their chiral order and $\rho \equiv \rho(s) = \sigma(s)/32\pi$. Then,

$$\begin{aligned} A &= e^{i\delta}\sqrt{(A_2 + \mathrm{Re}(A_4))^2 + \rho^2 T_2^2 A_2^2} \\ &= A_2 + \mathrm{Re}(A_4) + i\delta_2 A_2 + \mathcal{O}(p^6). \end{aligned} \tag{C2}$$

Comparing the two equations, we obtain that

$$\delta_2 = \rho T_2. \tag{C3}$$

A similar calculation can be done for $\pi\pi$ scattering PWAs that we denote as T. Given the corresponding element of the S matrix, $S = e^{2i\delta} = 1 + 2i\rho T$, with

$$T = \frac{1}{\rho} e^{i\delta} \sin\delta. \tag{C4}$$

By matching its perturbative expansions, $T = T_2 + T_4 + \mathcal{O}(p^6)$, to $\delta = \delta_2 + \delta_4 + \mathcal{O}(p^6)$, one obtains

$$\delta_2 = \rho T_2, \tag{C5}$$

$$\delta_4 = \rho \mathrm{Re} T_4. \tag{C6}$$

These are the expressions employed to obtain the ChPT phase shifts in Fig. 1.

APPENDIX D: COMPARISON WITH REF. [85]

A similar approach to treating the $a\pi \leftrightarrow \pi\pi$ rate below T_c was followed in Ref. [85] that appeared concurrently with our work. This analysis uses a different chiral rotation of the quark fields to transfer the $aG\tilde{G}$ term into the quark mass matrix in which the derivative axion coupling to the pion axial current vanishes and the complete axion-pion interactions are recovered by the rotation of the $a - \pi^0$ fields to the mass basis.

In this framework it becomes clear that up to chiral-symmetry-breaking terms $\propto m_\pi^2$, one can obtain the $a\pi \to \pi\pi$ scattering amplitude by rescaling the strong $\pi^0\pi \to \pi\pi$ amplitudes with the corresponding mixing angle $\theta_{a\pi} = 3C_{a\pi} f_\pi / 2 f_a$. Reference [85] then used this observation to obtain the axion-pion rates implementing amplitudes stemming from a set of Roy equations and dispersion-relation constraints calculated in Ref. [86]. In comparison with a unitarization of the full NLO chiral amplitude such as the one developed in this paper, this procedure misses $\mathcal{O}(m_\pi^2/s)$ corrections that are expected to be important only at small energies (or temperatures).

In Fig. 11 we illustrate this by comparing the results obtained for the different channels using the full NLO calculation of $a\pi \to \pi\pi$ in ChPT or using the NLO

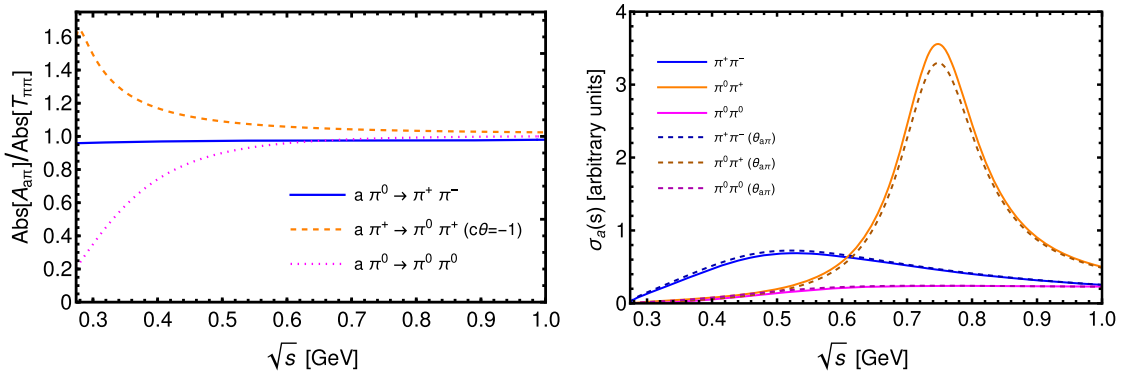

FIG. 11. Comparison of the amplitudes and cross sections for the full NLO ChPT calculation of $a\pi \to \pi\pi$ (amplitude denoted by $A_{a\pi}$) and for the NLO ChPT calculation of $\pi^0\pi \to \pi\pi$ rescaled by $\theta_{a\pi}$ (amplitude denoted by $T_{\pi\pi}$). In the left panel we show the ratio of the absolute values of the amplitudes, while in the right panel we show a comparison of the cross sections unitarizing the corresponding perturbative amplitudes with IAM.

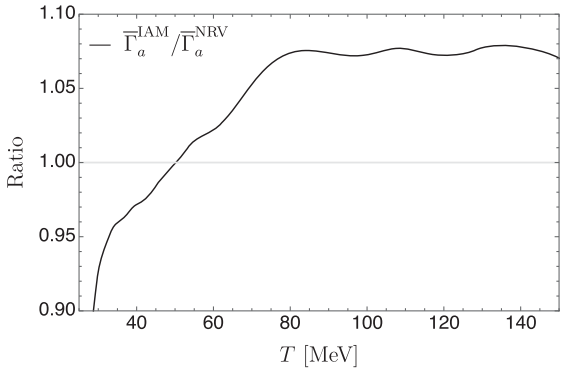

FIG. 12. Ratio between the IAM rate computed in this work and the $\bar{\Gamma}$ defined in Ref. [85]. To be uniform with the $\bar{\Gamma}$ definition in Ref. [85], here we show the IAM rate integrated with the modified Boltzmann factors $e^{-E_a/T} f_2(1+f_3)(1+f_4)$.

calculation of $\pi^0\pi \to \pi\pi$ scattering [36] multiplied by the mixing angle $\theta_{a\pi}$. From the left panel, showing the ratio of the amplitudes in the two methods, we observe that the $\mathcal{O}(m_\pi^2/s)$ corrections to the $a\pi^+ \to \pi^0\pi^+$ and $a\pi^0 \to \pi^0\pi^0$ are quite significant, up to 50–75% for $\sqrt{s} \lesssim 0.5$ GeV, while they are small (of order 5% in the same energy range) for the $a\pi^0 \to \pi^-\pi^+$ channel.[4] However, for $\sqrt{s} \lesssim 0.5$ GeV, the $\pi^0\pi^+$ and $\pi^0\pi^0$ channels are subdominant with respect to $\pi^+\pi^-$, and thus the differences in the total rate are small.

This is observed in the right panel of Fig. 11 where we show the total cross sections obtained for the different channels in the IAM using as perturbative input the full NLO ChPT calculation or the one derived from NLO ChPT of $\pi^0\pi \to \pi\pi$ rescaled by $\theta_{a\pi}$. In Fig. 12 we compare the full thermal rates in the two approaches, where we show that they agree within 8% (with higher discrepancy at higher T) in the temperature range between 40 and 150 MeV. This translates into a maximum 10% difference in the instantaneous decoupling temperature.

One could use different nonperturbative methods that at low energies recover the chiral expansion up to some order in ChPT and end up with unitarized PWAs with the correct analytical properties [28]. A full analysis of the differences in the prediction of the rate with the IAM method is beyond the scope of our work. However, let us briefly discuss the differences stemming from using another popular approach called the N/D method [67] in meson-meson, meson-baryon, and baryon-baryon scattering. A figure of merit in the comparison between IAM and N/D in these cases is the spread in the central values of the pole positions of the σ and $\rho(770)$ resonances at different orders and in different numbers of flavors of ChPT. For the σ we have a spread in the real and imaginary parts of the pole position in $\sqrt{s}$ of only 1.2% and 2.4%, respectively. We have taken the pole positions reported by applying, on the one hand, the IAM implemented from the NLO SU(2) [46], NNLO SU(2) [87], and NLO SU(3) ChPT [46,48] and, on the other hand, the N/D method applied from the NLO SU(2) [69], NNLO U(3) [88], and tree-level ChPT [89]. Similarly, for the $\rho(770)$ pole position in the $\sqrt{s}$ plane we find less than 1% and 2.7% of spread for the real and imaginary parts of the pole positions, respectively. Here we have taken the pole positions from Refs. [46,48,88]. These variations are representative of the differences one typically encounters between different methods to unitarize ChPT and we take them as indicative of the corresponding uncertainties in our approach. Note that these estimates are smaller than the uncertainties due to the variation of the cutoff discussed in Sec. VI.

[4]For instance, note that in the basis of Ref. [85] the rotation by $\theta_{a\pi}$ generates an $a\pi^0 \to \pi^0\pi^0$ term from the LO $m_\pi^2/f_\pi^2(\pi^0)^4$ term in the Lagrangian. This term would be canceled in the full calculation by an $a(\pi^0)^3$ piece directly stemming from the quark mass term. Related to this, the error estimate $\mathcal{O}(m_\pi^2/s)$ from Ref. [85] for $a\pi^0 \to \pi^0\pi^0$ falls short for this case because it really scales as $\mathcal{O}(m_\pi^2(4\pi f_\pi)^2/s^2)$, which in the effective field theory region of convergence is not small.

[1] R. D. Peccei and H. R. Quinn, Phys. Rev. Lett. **38**, 1440 (1977).
[2] R. D. Peccei and H. R. Quinn, Phys. Rev. D **16**, 1791 (1977).
[3] F. Wilczek, Phys. Rev. Lett. **40**, 279 (1978).
[4] S. Weinberg, Phys. Rev. Lett. **40**, 223 (1978).
[5] J. Preskill, M. B. Wise, and F. Wilczek, Phys. Lett. **120B**, 127 (1983).
[6] L. F. Abbott and P. Sikivie, Phys. Lett. **120B**, 133 (1983).
[7] M. Dine and W. Fischler, Phys. Lett. **120B**, 137 (1983).
[8] R. L. Davis, Phys. Lett. B **180**, 225 (1986).
[9] M. S. Turner, Phys. Rev. Lett. **59**, 2489 (1987); **60**, 1101(E) (1988).
[10] N. Aghanim *et al.* (Planck Collaboration), Astron. Astrophys. **641**, A1 (2020).
[11] N. Aghanim *et al.* (Planck Collaboration), Astron. Astrophys. **641**, A6 (2020).
[12] K. N. Abazajian *et al.* (CMB-S4 Collaboration), arXiv:1610.02743.
[13] E. Masso, F. Rota, and G. Zsembinszki, Phys. Rev. D **66**, 023004 (2002).
[14] P. Graf and F. D. Steffen, Phys. Rev. D **83**, 075011 (2011).

[15] Z. Berezhiani, A. Sakharov, and M. Khlopov, Sov. J. Nucl. Phys. **55**, 1063 (1992).
[16] S. Chang and K. Choi, Phys. Lett. B **316**, 51 (1993).
[17] S. Hannestad, A. Mirizzi, and G. Raffelt, J. Cosmol. Astropart. Phys. 07 (2005) 002.
[18] F. D'Eramo, F. Hajkarim, and S. Yun, Phys. Rev. Lett. **128**, 152001 (2022).
[19] F. D'Eramo, F. Hajkarim, and S. Yun, J. High Energy Phys. 10 (2021) 224.
[20] Y. Aoki, Z. Fodor, S. D. Katz, and K. K. Szabo, Phys. Lett. B **643**, 46 (2006).
[21] S. Borsanyi, Z. Fodor, C. Hoelbling, S. D. Katz, S. Krieg, C. Ratti, and K. K. Szabo (Wuppertal-Budapest Collaboration), J. High Energy Phys. 09 (2010) 073.
[22] A. Bazavov *et al.*, Phys. Rev. D **85**, 054503 (2012).
[23] L. Caloni, M. Gerbino, M. Lattanzi, and L. Visinelli, J. Cosmol. Astropart. Phys. 09 (2022) 021.
[24] F. D'Eramo, E. Di Valentino, W. Giarè, F. Hajkarim, A. Melchiorri, O. Mena, F. Renzi, and S. Yun, J. Cosmol. Astropart. Phys. 09 (2022) 022.
[25] L. Di Luzio, G. Martinelli, and G. Piazza, Phys. Rev. Lett. **126**, 241801 (2021).
[26] H. Lehmann, Phys. Lett. **41B**, 529 (1972).
[27] T. N. Truong, Phys. Rev. Lett. **61**, 2526 (1988).
[28] J. A. Oller, Symmetry **12**, 1114 (2020).
[29] H. Georgi, D. B. Kaplan, and L. Randall, Phys. Lett. **169B**, 73 (1986).
[30] L. Di Luzio, M. Giannotti, E. Nardi, and L. Visinelli, Phys. Rep. **870**, 1 (2020).
[31] J. E. Kim, Phys. Rev. Lett. **43**, 103 (1979).
[32] M. A. Shifman, A. I. Vainshtein, and V. I. Zakharov, Nucl. Phys. **B166**, 493 (1980).
[33] A. R. Zhitnitsky, Yad. Fiz. **31**, 497 (1980) [Sov. J. Nucl. Phys. **31**, 260 (1980)].
[34] M. Dine, W. Fischler, and M. Srednicki, Phys. Lett. **104B**, 199 (1981).
[35] L. Di Luzio and G. Piazza, J. High Energy Phys. 12 (2022) 041.
[36] J. Gasser and H. Leutwyler, Ann. Phys. (N.Y.) **158**, 142 (1984).
[37] H. Lehmann, K. Symanzik, and W. Zimmermann, Nuovo Cimento **1**, 205 (1955).
[38] G. Colangelo, J. Gasser, and H. Leutwyler, Nucl. Phys. **B603**, 125 (2001).
[39] Y. Aoki *et al.* (Flavour Lattice Averaging Group (FLAG)), Eur. Phys. J. C **82**, 869 (2022).
[40] G. Grilli di Cortona, E. Hardy, J. Pardo Vega, and G. Villadoro, J. High Energy Phys. 01 (2016) 034.
[41] P. Zyla *et al.* (Particle Data Group), Prog. Theor. Exp. Phys. **2020**, 083C01 (2020).
[42] J. A. Oller, Prog. Part. Nucl. Phys. **110**, 103728 (2020).
[43] K. M. Watson, Phys. Rev. **88**, 1163 (1952).
[44] J. R. Pelaez, Phys. Rep. **658**, 1 (2016).
[45] J. A. Oller, *A Brief Introduction to Dispersion Relations*, SpringerBriefs in Physics (Springer, New York, 2019).
[46] A. Dobado and J. R. Pelaez, Phys. Rev. D **56**, 3057 (1997).
[47] J. A. Oller and E. Oset, Nucl. Phys. **A620**, 438 (1997); **A652**, 407(E) (1999).
[48] J. A. Oller, E. Oset, and J. R. Pelaez, Phys. Rev. D **59**, 074001 (1999); **60**, 099906(E) (1999); **75**, 099903(E) (2007).
[49] J. Nieves and E. Ruiz Arriola, Phys. Lett. B **455**, 30 (1999).
[50] A. Dobado, M. J. Herrero, and T. N. Truong, Phys. Lett. B **235**, 134 (1990).
[51] T. N. Truong, Phys. Rev. Lett. **67**, 2260 (1991).
[52] A. Dobado and J. R. Pelaez, Phys. Rev. D **47**, 4883 (1993).
[53] A. Salas-Bernárdez, F. J. Llanes-Estrada, J. Escudero-Pedrosa, and J. A. Oller, SciPost Phys. **11**, 020 (2021).
[54] R. L. Workman (Particle Data Group), Prog. Theor. Exp. Phys. **2022**, 083C01 (2022).
[55] S. J. Lindenbaum and R. S. Longacre, Phys. Lett. B **274**, 492 (1992).
[56] P. Estabrooks and A. D. Martin, Nucl. Phys. **B79**, 301 (1974).
[57] M. J. Losty, V. Chaloupka, A. Ferrando, L. Montanet, E. Paul, D. Yaffe, A. Zieminski, J. Alitti, B. Gandois, and J. Louie, Nucl. Phys. **B69**, 185 (1974).
[58] W. Hoogland *et al.*, Nucl. Phys. **B126**, 109 (1977).
[59] J. R. Batley *et al.* (NA48/2 Collaboration), Eur. Phys. J. C **54**, 411 (2008).
[60] C. D. Froggatt and J. L. Petersen, Nucl. Phys. **B129**, 89 (1977).
[61] W. Ochs, Ph.D. thesis, University of Munich, 1974.
[62] B. Hyams *et al.*, Nucl. Phys. **B64**, 134 (1973).
[63] S. D. Protopopescu and *et al.*, Phys. Rev. D **7**, 1279 (1973).
[64] P. Estabrooks and *et al.*, AIP Conf. Proc. **13**, 37 (1973).
[65] G. Grayer and *et al.*, *Proceedings of the 3rd Philadephia Conference on Experimental Meson Spectroscopy* (American Institute of Physics, Philadephia, New York, 1972).
[66] R. Kaminski, L. Lesniak, and K. Rybicki, Z. Phys. C **74**, 79 (1997).
[67] J. A. Oller and E. Oset, Phys. Rev. D **60**, 074023 (1999).
[68] G. Janssen, B. C. Pearce, K. Holinde, and J. Speth, Phys. Rev. D **52**, 2690 (1995).
[69] M. Albaladejo and J. A. Oller, Phys. Rev. D **86**, 034003 (2012).
[70] F. Guerrero and J. A. Oller, Nucl. Phys. **B537**, 459 (1999); **B602**, 641(E) (2001).
[71] J. Gasser and H. Leutwyler, Phys. Lett. B **184**, 83 (1987).
[72] J. Gasser and H. Leutwyler, Phys. Lett. B **188**, 477 (1987).
[73] P. Gerber and H. Leutwyler, Nucl. Phys. **B321**, 387 (1989).
[74] S. Hannestad and J. Madsen, Phys. Rev. D **52**, 1764 (1995).
[75] H. Leutwyler, in *Proceedings of the 5th International Workshop on Chiral Dynamics, Theory and Experiment* (2006), arXiv:hep-ph/0612112.
[76] E. W. Kolb and M. S. Turner, *The Early Universe* (CRC Press, London, 1990), Vol. 69.
[77] K. Saikawa and S. Shirai, J. Cosmol. Astropart. Phys. 05 (2018) 035.
[78] L. Di Luzio, M. Giannotti, F. Mescia, E. Nardi, S. Okawa, and G. Piazza, arXiv:2305.11958.
[79] L. Darmé, L. Di Luzio, M. Giannotti, and E. Nardi, Phys. Rev. D **103**, 015034 (2021).
[80] A. Hook, Phys. Rev. Lett. **120**, 261802 (2018).
[81] L. Di Luzio, B. Gavela, P. Quilez, and A. Ringwald, J. High Energy Phys. 05 (2021) 184.
[82] L. Di Luzio, B. Gavela, P. Quilez, and A. Ringwald, J. Cosmol. Astropart. Phys. 10 (2021) 001.
[83] A. Gomez Nicola, F. J. Llanes-Estrada, and J. R. Pelaez, Phys. Lett. B **550**, 55 (2002).
[84] A. Dobado, A. Gomez Nicola, F. J. Llanes-Estrada, and J. R. Pelaez, Phys. Rev. C **66**, 055201 (2002).

[85] A. Notari, F. Rompineve, and G. Villadoro, Phys. Rev. Lett. **131**, 011004 (2023).
[86] R. Garcia-Martin, R. Kaminski, J. R. Pelaez, J. Ruiz de Elvira, and F. J. Yndurain, Phys. Rev. D **83**, 074004 (2011).
[87] T. Hannah, Phys. Rev. D **60**, 017502 (1999).
[88] Z.-H. Guo, J. A. Oller, and J. Ruiz de Elvira, Phys. Rev. D **86**, 054006 (2012).
[89] M. Albaladejo and J. A. Oller, Phys. Rev. Lett. **101**, 252002 (2008).